CEAS Space Journal
https://doi.org/10.1007/s12567-025-00637-4

ORIGINAL PAPER

Investigation of a coaxial pulsed plasma thruster by electrothermal discharge in Teflon propellant

M. M. Abo El-Hadeed[1] · M. E. Abdelkader[2] · F. B. Diab[2] · M. A. Abd Al-Halim[1]

Received: 25 March 2025 / Revised: 29 May 2025 / Accepted: 10 June 2025

Abstract
The simplicity, efficiency, and reliability of pulsed plasma thrusters make them a preferred choice in low-power systems for microsatellites. In this paper, a coaxial electrothermal pulsed plasma thruster was designed and tested using Teflon as a solid propellant. The ablated mass was measured for different values of peak discharge current and number of pulses. The Experimental results of our system were compared with calculated values obtained using a 1-D time-dependent ETFLOW model for the electrothermal capillary system. The model was used to calculate the values of thrust and impulse for each case. Experimentally, increasing the number of pulses resulted in an increase in the total ablated mass and the capillary diameter. Experimentally, increasing the peak discharge current from 1.95 kA to 5.66 kA led to an increase in the ablated mass per pulse from 128.4 μg to 980.8 μg and the impulse from 340 μN.s to 2156 μN.s. In addition, extending the capillary length from 3 to 8 cm led to an increase in the ablated mass from 52 μg to 326.2 μg, consistent with the calculated data. Moreover, the thrust efficiency was investigated as a function of input energy and capillary length. The maximum achieved thrust efficiency was about 8.9% for an input energy of 6 J and a capillary length of 6 cm. Theoretically, the model predicted that thrust, impulse, and specific impulse increase with raising the peak discharge current.

Keywords PPT · Electrothermal discharge · Ablated mass · Thrust · Impulse · Specific impulse

1 Introduction

Worldwide interest in micro- and nano-satellites has been increasing due to their low cost and versatility, which make them suitable propulsion systems used in space exploration and interplanetary missions, such as station-keeping, maneuvering, and attitude control [1, 2]. Seeking advantages such as simplicity, stability, robustness, reliability, and low energy consumption, electric propulsion systems, especially Pulsed Plasma Thrusters (PPTs), have emerged as preferred alternative engines for small satellites rather than the chemical thrusters [3]. Although chemical thrusters can achieve higher thrust values, electric thrusters utilize less propellant, producing small thrust over a long duration [4]. In addition, PPTs work with variable thrust and specific impulse stages and can provide small, discrete values of impulse [5, 6]. In contrast, PPTs suffer from some disadvantages, such as limited specific impulse and late-time ablation, which decreases the propellant utilization [7, 8].

Although Electrothermal PPTs (ETPPTs) suffer from low specific impulse [9], they emerged as high-thrust electric propulsion systems, achieving higher thrust levels than electromagnetic engines [10]. The thrust mechanism in ETPPTs depends on the thermal expansion of the generated plasma. The performance of many propellants; solid, liquid, and gas types has been tested. To achieve a high reliability and light weight system, solid propellants are preferred since they do not require a storage system and eliminate propellant leakage. Teflon is the most widely used solid propellant due to its ability to resist fire and corrosion, which make it suitable for high-temperature, long-duration operation [11]. In solid ablative ETPPTs, the energy stored in the capacitor bank is discharged between the two electrodes along the surface of the propellant, and due to temperature, a portion of the propellant is dissociated, ionized, then it forms plasma, which is accelerated by the pressure gradient, generating thrust.

✉ M. M. Abo El-Hadeed
marwa.aboelhadeed@fsc.bu.edu.eg

[1] Physics Department, Faculty of Science, Benha University, Benha 13518, Egypt

[2] Plasma & Nuclear Fusion Dept, Nuclear Research Centre, Egyptian Atomic Energy Authority, Cairo 13759, Egypt

Published online: 25 June 2025

The performance of capillary ETPPTs is influenced by many factors, such as the capillary length, capillary diameter, and input voltage. Many studies were conducted on the capillary ET system to study its performance. T. Edamitsu and H. Tahara [12] investigated the performance of capillary-based ET thrusters with different values of capillary length in a range of 4 mm to 34 mm. It was shown that a longer cavity can achieve higher values of impulse, and this is in agreement with other researches [8] in which the mass shot per joule increases from 6.5 μg/J to 11 μg/ J with increasing capillary length from 8 to 12 mm. In addition, increasing the input voltage will raise the value of ablated mass, impulse, and specific impulse. In contrast, increasing the capillary diameter from 3 to 5 mm, the mass shot per joule decreased from 6.5 to 4.2 μg/J. which agrees with [13]. In addition, an endurance test was conducted by measuring the impulse values during 40,000 pulses. The impulse value decreases by increasing the number of shots [10]. Moreover, the impulse value was measured using a pendulum method where a small target was located close to the nozzle [4].

There are many models that have been developed to characterize the electrothermal designs. Keidar et al. developed a time-dependent model to study the electrothermal plasma thruster properties using a Teflon capillary [14]. Their model distinguished two layers between the inner Teflon wall and the arc plasma: the collision-dominated hydrodynamic layer and the kinetic Knudsen layer. The model underpredicted the experimental results of ablated mass by about 25%. However, the calculated ablated mass and impulse had the same behavior as measured, increasing for longer cavity length and decreasing for larger cavity diameter [15]. Similarly, Edamitsu et al. conducted an unsteady state simulation of electrothermal discharge with Teflon propellant, taking into consideration that the plasma is in local thermodynamic equilibrium and exhibits only single ionization [10]. Their model showed good agreement between their calculated and experimental ablated mass, although their impulse calculations were slightly higher than experimental results [10]. Also, Cambier et al. established a zero-dimensional model to characterize the discharge properties of a polyethylene capillary [16]. The model includes the effect of high-density non-ideal plasma effects, and it assumes that the plasma is in LTE and the ablated mass is fully ionized. It was found that increasing voltage improved impulse and thrust, while longer capillaries let to a reduction in specific impulse [16].

In this research, a capillary electrothermal PPT is constructed using a Teflon propellant of long tubes up to 6cm. The ablated mass per pulse is measured with different peak currents. In addition, the ablated mass and impulse were measured as a function of the capillary length and diameter. The relationship between the number of pulses and ablated mass per pulse was measured during 5000 pulses. The experimental data were compared with calculated values obtained using ETFLOW modeling [17–22]. The model is used to study the variation of thrust with discharge time and to calculate various discharge parameters such as velocity, heat flux, plasma density, and pressure, as functions of capillary length and discharge current.

2 Experimental setup

Figure 1 shows a schematic diagram of the electrothermal capillary PPT system. It consists of a glass vacuum chamber of 27 cm in height and 23 cm in diameter and two electrodes, an annular ring cathode connected to an extended copper body with an inner diameter of 3 cm and a rod anode of 4 mm diameter, which is shielded by polyacrylic as an insulator, and an anode tip is 1 cm in long. Between the two electrodes, an insulating material with an inner diameter of 1.7 cm serves as a host for the propellant. The whole system is evacuated using a mechanical rotary pump.

Figure 2 illustrates the electric circuit to which the system is connected, while Table 1 presents the experimental parameters used in this study by varying the applied input. The circuit consists of a DC power supply, a capacitor bank with a total capacitance of 5.32 μF, and an air gap switch. A Rogowski coil is connected to an integrator circuit and an oscilloscope to measure the discharge current. The used coil is 109 turns, with a major diameter of 4.5 cm, and an inner diameter of is 4 mm for each turn. The coil is connected to an RC integrator circuit, and the charging voltage

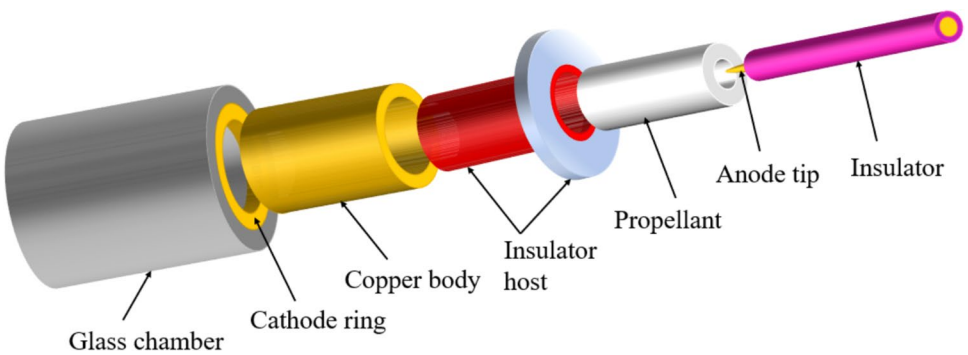

Fig. 1 The components of the electrothermal capillary system

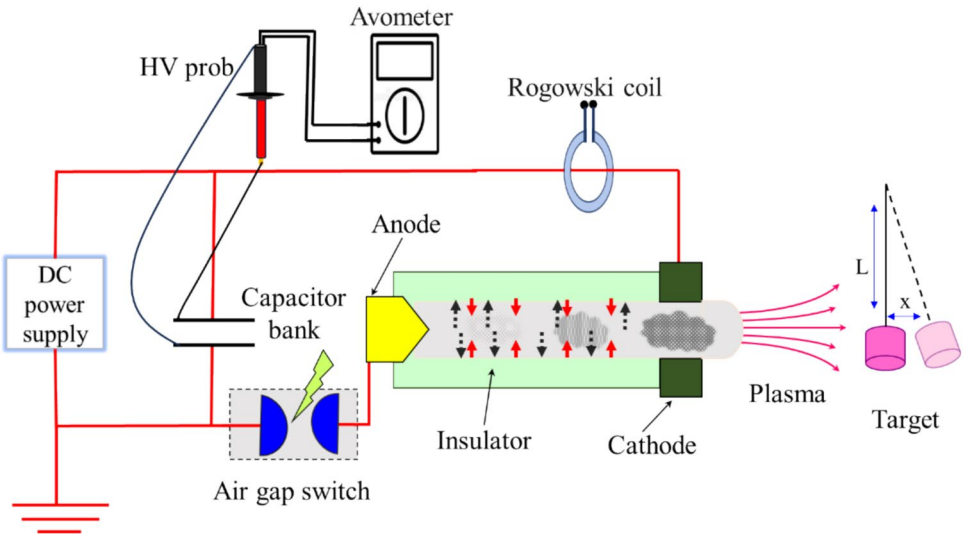

Fig. 2 The electrical circuit connected to the system

Table 1 The circuit parameters used in discharge

Initial voltage (kV)	1.5—4
Discharge current (kA)	1.95—5.66
Pulse duration (μs)	19
Capacitance (μF)	5.32
Capillary length (cm)	5
Capillary diameter (mm)	4
Material of capillary	Teflon

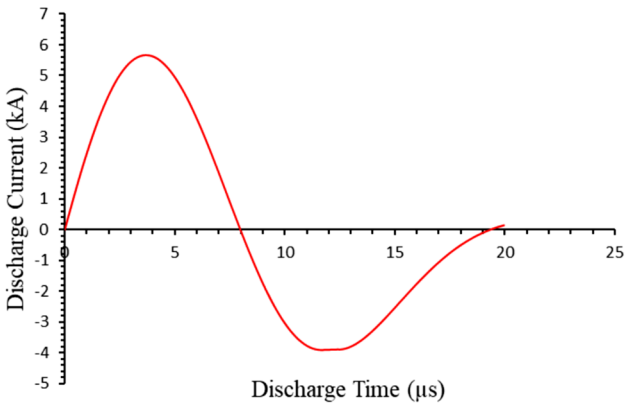

Fig. 3 Waveform of discharge current with input voltage of 4kV

is measured using a high-voltage probe. Besides, the impulse is measured using the pendulum method. A cylindrical target with a mass of 1 g is suspended by a string so that the mass is positioned in front of the nozzle. When plasma is expelled from the capillary, it pushes the target. By knowing the horizontal displacement of target and string length, the impulse could be calculated.

The system is a self-discharge one; capacitors discharge into the capillary through an air-gap switch, initiating an arc. The heat radiated from the discharge current via Joule heating is absorbed by the inner wall of the capillary propellant, causing ablation of the wall material [23, 24]. The dissociated atoms and molecules become ionized, forming high-density and high-pressure plasma inside the capillary. The plasma exits the capillary due to the high-pressure gradient, generating thrust. The amount of the ablated mass and the plasma exit velocity control the impulse generated by the thruster.

The ablated atoms from the walls form a dense vapor that can absorb part of the radiant energy and reduce the amount of energy that reaches the wall. Only a fraction of the heat flux is transmitted to the wall, and the arc is not assumed an ideal blackbody. Therefore, the ablated mass is affected by the value of the transmission heat factor (gray factor), which is less than one for the non-ideal blackbody radiation. This phenomenon is called the vapor shielding effect [25, 26].

Figure 3 shows the wave signal of the discharge current for an input voltage of 4 kV. The discharge current peak was measured using a Rogowski coil connected to an integrator circuit. The discharge current reaches a peak of 5.66 kA at 3.66 μs.

The next section addresses the effect of changing the applied voltage on the ablated mass and the effect of the capillary dimensions, such as length and diameter, on the values of ablated mass. The voltage was varied between 1.5 kV and 4 kV for a Teflon capillary of 5 cm long and 4 mm in diameter. The circuit's capacitance is 5.32 μF, and the pulse duration is 19 μs.

3 Theoretical considerations

The theoretical results were obtained using the ET FLOW modeling code, which provides a deep description of the essential physical parameters of the capillary Electrothermal system including, the plasma density, temperature, pressure, velocity, ablated mass, and internal energy. The model is based on several assumptions, which can be summarized as follows: the model is 1D, time-dependent. There is no effect due to the radial phase. Plasma is assumed to be in local thermodynamic equilibrium, and the ablated particles from the surface of the capillary partially absorb the incoming radiation. Only a fraction of heat flux reaches the wall. Ohmic heating is considered uniform in the capillary, while frictional forces and magnetic pressure are negligible, radiant heat transfer is dominant, and the capillary hollow radius remains constant [17, 18]. The basic equations to build this model include conservation of mass, momentum, and energy [19–21, 26], besides the thrust equations such as thrust, impulse, and specific impulse which can describe the thruster's performance.

The mass conservation equation indicates that the difference between the rate of ablation and the number density of particles which enter or leave the capillary is equal to the time rate of change of plasma density inside the capillary [17, 19–21]:

$$\frac{\partial n}{\partial t} = \dot{n} - \frac{\partial (vn)}{\partial z} \tag{1}$$

where n is the number density of the plasma (m^{-3}), v is the plasma velocity (m/s), and $\dot{n}$ is the rate of ablation ($m^{-3}.s^{-1}$). The momentum conservation equation could be given as:

$$\frac{\partial v}{\partial t} = -K_{Press} - K_{KE} - K_{dens} \tag{2}$$

where K_{Press} is for pressure gradient, K_{KE} is the gradient of kinetic energy, and K_{dens} is for change in density due to the ablation process. Also, the energy conservation equation can be given as:

$$n\frac{\partial U}{\partial t} = U_{joule} - U_{Rad} - U_{work} - U_{trans} \tag{3}$$

where U_{joule} is for joule heating, U_{Rad} is thermal radiation, U_{work} is the work done by plasma, and U_{trans} is loss due to particles entering or leaving the capillary.

The thrust (Γ) is the force responsible for propelling plasma. It is defined as the product of the mass flow rate multiplied by the exhaust velocity of plasma from the capillary end [27] and the impulse (I_m) is obtained by integrating the thrust [27] over the time of the pulse duration [28]:

$$\Gamma = \frac{dm}{dt}.v \tag{4}$$

$$I_m = \int \Gamma dt = v_{ex}\int_0^t \frac{dm}{dt}dt \tag{5}$$

The specific impulse I_s is defined as the impulse per unit weight of propellant [27]. and given by:

$$I_s = \frac{\int \Gamma dt}{g.\int_0^t \frac{dm}{dt}dt} \tag{6}$$

where: g is the acceleration due to gravity.

4 Results and discussion

The ablation rate could be described according to the energy of the radiation heat flux which is transferred to the capillary wall, causing material ablation. The rate of ablation $\dot{n}$ is given by:

$$\dot{n} = \frac{2q}{RH_{sub}A_P} \tag{7}$$

where H_{sub} is the specific heat of sublimation (J/kg), R is the capillary radius, A_p is the mass of the atom constitutes plasma (kg/atom), and q is radiation heat flux (W/m^2) [20, 21], which could be given by [17, 18]:

$$q = F_t\sigma_s\left(T^4 - {T_{vap}}^4\right) \tag{8}$$

where σ_s is Stefan – Boltzmann constant, T is plasma temperature, T_{vap} is the vaporization temperature of the capillary, and F_t is the energy transmission factor (gray factor) which for organic polymers such as Teflon and polyethylene can be given by [29]:

$$F_t = 1 - e^{-0.025(Pr)^{0.6}} \tag{9}$$

where: P is the pressure (in bar), and r is the arc radius (mm). It is assumed that the plasma fills all the capillary tubes, therefore $r \approx R$.

The radiation heat from the arc depends on the plasma temperature and transmission heat factor. For the ideal case, the transmission heat factor is equal to one, meaning that the radiation behaves as ideal blackbody radiation. However, because of the vapor-shielding effect caused by the ablated molecules, the transmission heat factor varies with the pressure inside the capillary and the arc radius. Increasing either the plasma temperature or transmission heat factor leads to a higher heat flux, thereby, enhancing the ablation process. In the next sections, we address various factors affecting the discharge and propulsion.

4.1 Discharge current

Figure 4 shows the variation in ablated mass as a function of the peak discharge current. Experimentally, increasing the peak current from 1.95 kA to 5.66 kA results in an increase in the ablated mass from 128.4 μg to 980.8 μg per pulse following the equation M[μg] = 231.79 I[kA]—370.93. A higher current leads to a rise in the temperature inside the capillary, which in turn increases the radiation heat flux on the inner surface of the capillary and thereby increases the ablated mass.

The calculated data using the ideal transmission heat factor $F_t = 1$, the mass increases with peak current from 285 μg to 1170 μg, which is greater than the experimental values. However, the calculated values using the transmission heat factor according to Eq. 9 show that the mass increases from 145 μg to 797 μg, which closely aligns with experimental data. The radiation from the arc is not purely ideal blackbody radiation because not all the radiation produced by the arc reaches the wall due to the vapor shielding effect, which is caused by dissociated atoms and molecules. This shielding prevents a part of the radiation from reaching the inner wall of the capillary, and allows only a fraction of incident radiation. As a result, the ideal transmission heat factor overestimates the ablated mass compared to the values measured experimentally.

Figure 5 shows the capillary diameter variation before and after 5000 pulses. Also, Fig. 6 shows the variation of total ablated mass and capillary diameter as a function of discharge pulses. Increasing the number of pulses increases the total ablated mass from 0.064 g after 500 pulses to 1.26 g after 5000 pulses, with an average ablated mass of 206.2 μg per pulse. As a result of this ablation, the capillary diameter became wider and increased from 4 mm to 5.5 mm. By measuring the ablated mass after a specified number of pulses, and assuming a uniform ablation along the length,

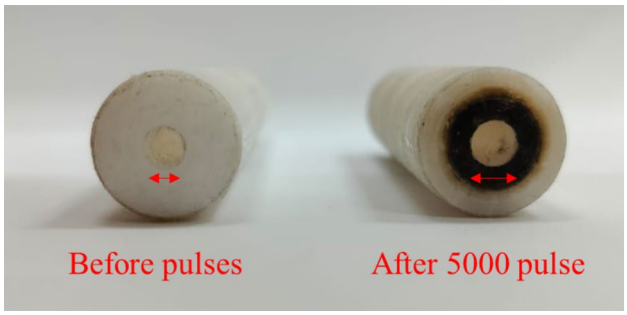

Fig. 5 The change in the capillary diameter due to the number of shots

the change in the capillary diameter as a function of the number of pulses can be calculated from the equations:

$$V = \frac{m}{\rho_t}, V = \frac{D^2}{4}\pi L \tag{10}$$

where D is the capillary diameter, ρ_t is the Teflon density (2.29 gm/ cm^3) and L is the capillary length.

Figure 7 shows the change in the peak heat flux, plasma density, pressure, and exit velocity with peak current. As the peak current increases from 1.95 kA to 5.66 kA, the heat flux radiated from the arc increases from 0.63 GW/m^2 to 3.3 GW/m^2 following the power law Q[GW/m^2] = 0.22 I[kA]$^{1.56}$, as a result, the ablation of propellant increases accompanied by a rise in plasma density from 0.11 kg/m^3 to 0.62 kg/m^3 following the power law ρ [kg/m^3] = 0.039 I[kA]$^{1.5814}$. Increasing plasma density increases the pressure inside the capillary from 5.1 bar to 31 bar following the power law of P[bar] = 1.63 I[kA]$^{1.69}$. Also, the exit velocity increases from 2.85 km/s to 3.15 km/s following the scaling law v[km/s] = 0.078 I[kA] + 2.72. Increasing the input current leads to a rise in temperature inside the capillary which

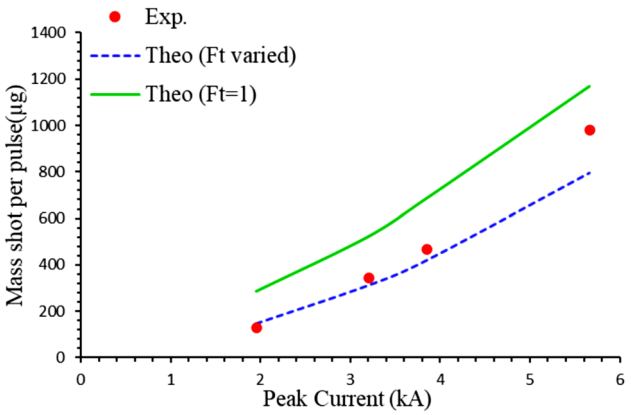

Fig. 4 Change in ablated mass with peak current

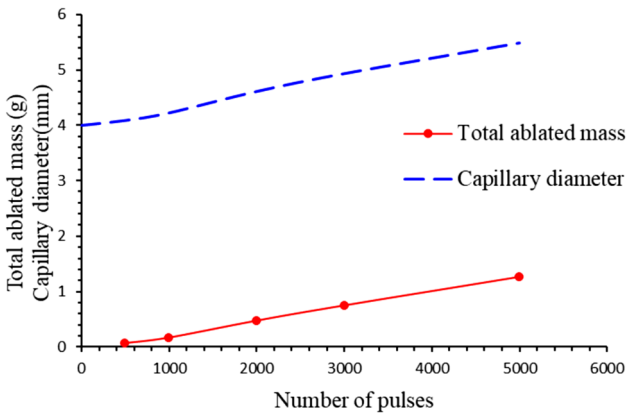

Fig. 6 The change in total ablated mass and capillary diameter with the number of shots

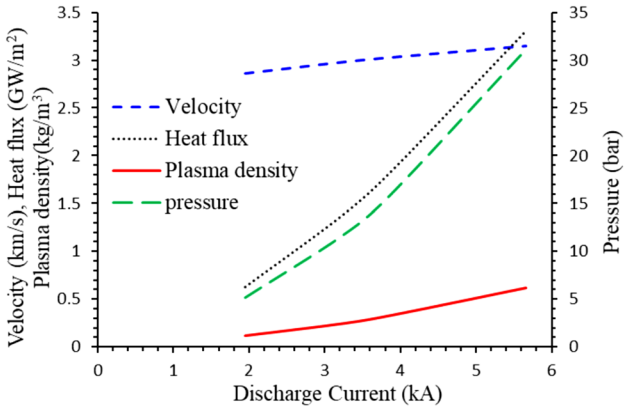

Fig. 7 Increasing the peak of heat flux, plasma density, pressure, and exit velocity with increasing the peak current

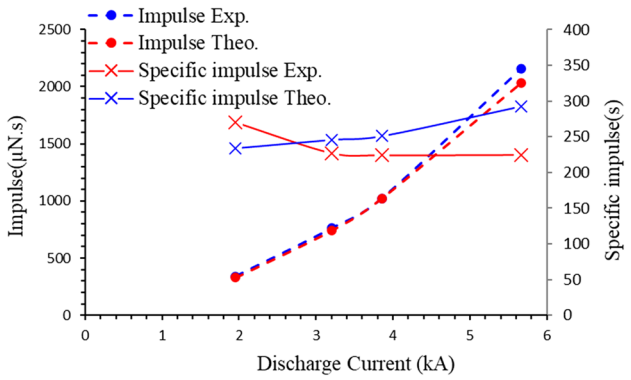

Fig. 9 Change in measured and calculated impulse and specific impulse with discharge current

in turn increases the kinetic energy of plasma species, hence, the exit velocity increases.

It is shown that with increasing the number of pulses; the capillary diameter increases and the ablation rate tends to reduce as the capillary diameter increases with increasing the number of pulses. An increase in capillary diameter reduces the energy density, i.e., reduces the incident heat flux reaches the inner wall, which leads to decreases the ablation rate.

Figure 8 shows the change in calculated thrust profiles with different input voltages. The peak thrust increases from 47.6 N to 278 N by increasing as the discharge current peak rises from 1.95 kA to 5.66 kA. All curves reach the peak thrust simultaneously at 5.5 μs and vanish by the end of discharge. Increasing the input current leads to a rise in the radiation heat flux from the arc, and this, according to Eq. 7, increases the ablation rate from the capillary and enhances the exit velocity. Consequently, the thrust values are increased, as shown in Eq. 4.

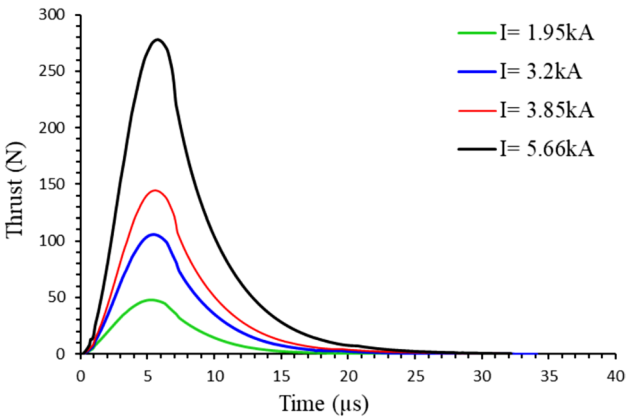

Fig. 8 Thrust profile for different discharge current

Figure 9 shows the change in measured and calculated impulse values, as well as the specific impulses as a function of the peak discharge current value. The impulse was measured experimentally using the pendulum method [4]. Experimentally, as the peak current increased from 1.95 kA to 5.66 kA, the impulse rises from 340 μN.s to 2156 μN.s [8, 10]. The specific impulse decreasing from 270 to 226s for discharge current of 3.2 kA, then increasing the current to about 5.66 kA does not significantly affect the values. Theoretically, the impulse increases from 330 μN.s to 2033 μN.s, which is in good agreement with experimental data, while the specific impulse increased from 234 s to 292.7 s [8, 10]. Increasing the discharge current peak enhances the ablation due to the temperature rise, which in turn increases the exit velocity of the plasma, according to the thrust equation Eq. 4. Thrust increases with both the ablated mass and exit velocity, which increases impulse as well, according to Eq. 5.

From the previous discussion, increasing the discharge current, results in a higher heat flux, and temperature incident on the inner wall of the capillary are also increased. As a result, the ablation process increased, accompanied by an increase in impulse. In addition, increasing the ablation process raises the plasma density inside the capillary; hence, the pressure is also increased. Moreover, as the temperature and pressure are rising inside the capillary, the kinetic energy of the plasma species also increases, which in turn increases velocity and impulse.

4.2 Capillary length

Figure 10 shows the change in the ablated mass and heat flux with capillary length for a peak discharge current of 1.95 kA using Eq. 9 for calculating the transmission heat factor, as it produces results in good agreement with experimental measurements. Experimentally, the ablated mass increases from 52 μg to 158 μg as the capillary length

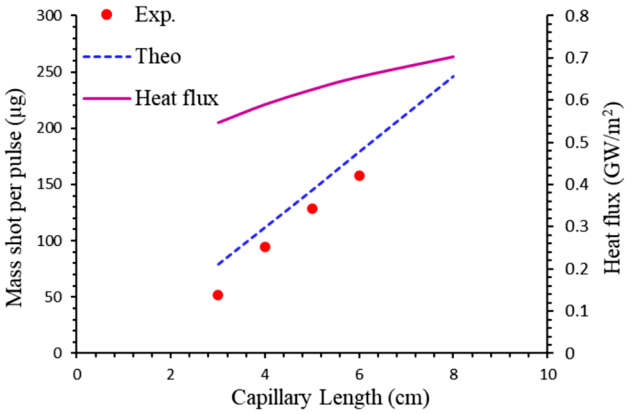

Fig. 10 The change in ablated mass as a function of capillary length

increased from 3 to 6 cm following the linear relation of M[µg] = 35.22 L[cm] – 50.34. The calculated data follows the same trend where the ablated mass increased from 79 µg to 179 µg. The heat flux also increases from 0.55 GW/m^2 to 0.66 GW/m^2 following the scaling law of $Q\left[\frac{GW}{m^2}\right] = 0.16\ln(L[cm]) + 0.38$. The longer capillaries have wider area exposed to radiation flux, which leading to higher ablation rates and greater ablated mass [8]. According to Eq. 8, the heat flux is proportional to the fourth power of the temperature, so it increases even with the slight increase of the temperature.

The plasma state is described by a modified Saha equation, which explains the relationship between the ionization potential and the effective charge state using the equation [26]:

$$I_i\left(Z_{eff} + 0.5\right) = K_B T \ln\left(\frac{AT^{1.5}}{Z_{eff} n}\right) \tag{11}$$

Hence I_i is the ionization potential and A is constant.

The pressure (P) inside the capillary can be determined using the equation of state [17, 18]:

$$P = nK_B T(1 + Z_{eff}) \tag{12}$$

where Z_{eff} is the effective charge state which is given as [17, 18]:

$$Z_{eff} = \frac{\sum_j Z_j^2 n_j}{n_e} \tag{13}$$

where j refers to the ion species of charge state z, and n_e is the density of electrons and the summation over the ions only.

The equations explain the effects of both the temperature and ion species on pressure, which in turn affects the ablation rate and the thrust properties. Increasing the plasma temperature leads to a higher ionization of plasma species, consequently enhancing the ablation rate from the capillary wall. This rises the pressure inside the capillary, consequently increasing the thrust and impulse values.

Figure 11 shows the variation of plasma and ion number density as a function of the capillary length for a peak current of 1.95 kA. By increasing the capillary length from 3 to 6 cm, the ablation increases leading to a rise in plasma density from 0.1 kg/m^3 to 0.12 kg/m^3 and an increase in the ion number density from 4.85×10^{23} m^{-3} to 6.41×10^{23} m^{-3} following the power equation $n_i\,[m^{-3}] = 3 \times 10^{23}\,L[cm]^{0.4011}$. The increase in plasma and ion number density with capillary length is related to the greater area exposed to the heat, which enhances the ability of heat flux to ablate more layers from the inner capillary wall.

The variation of plasma exit velocity and pressure with the capillary length is illustrated in Fig. 12. According to Eq. 12, a rise in peak pressure accompanies the increase

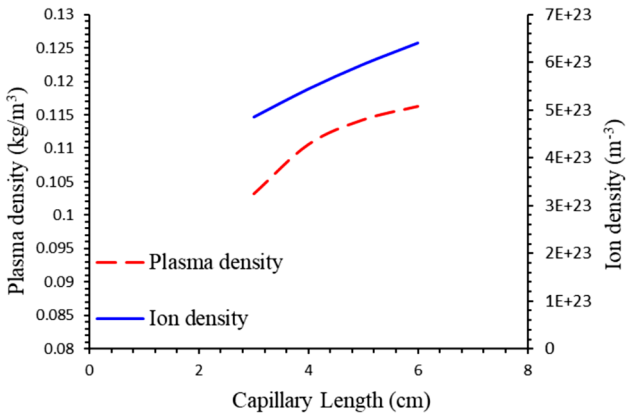

Fig. 11 Plasma density and ion density variation with the capillary length

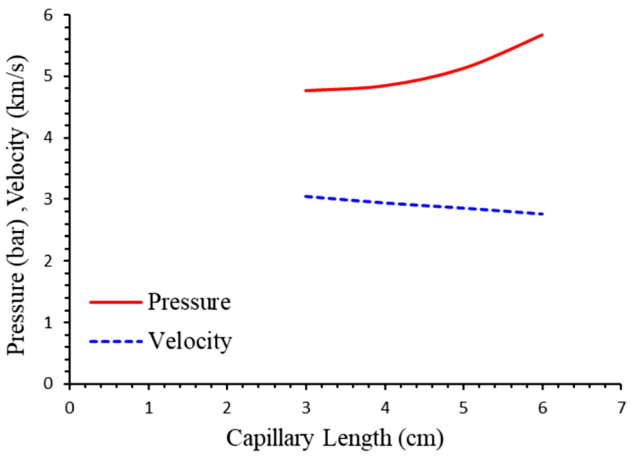

Fig. 12 The variation of pressure and velocity with the capillary length

in ion density. The peak pressure increases from 4.77 bar to 5.68 bar following the fitting equation P[bar] = 0.12 L[cm]^2—0.75 L[cm] + 5.97. On the other hand, extending the capillary length decreases the plasma exit velocity from 3 km/s to 2.8 km/s, following the linear equation v[km/s] = -0.094 L[cm] + 3.32. The reduction in velocity is related to the change in pressure according to Eq. 2, and is also affected by the higher ablated mass, which increases the drag force.

Figure 13 shows the variation of the thrust profile as a function of the capillary length. Increasing the capillary length from 3 to 6 cm increases the peak thrust per pulse from 33.3 N to 53N, taking into account that all curves have the same pulse width. Thrust begins to increase with the ablation process until it reaches its maximum value, after which it gradually decreases and vanishes by the end of the discharge. Increasing capillary length enhances the ablation rate and ion number density, causing a rise in thrust values according to Eq. 4 [16].

Figure 14 shows the change in measured and calculated impulse as a function of capillary length. By increasing the capillary length from 3 to 6 cm, the ablation rate increases due to the larger area exposed to heat. As a result, the measured impulse increases from 173 μN.s to 464.5 μN.s following the linear equation of I_m [μN.s] = 80.1 L[cm]—67.2, which is in good agreement with calculated values in which the impulse increased from 202 μN.s to 480 μN.s. In contrast, increasing the capillary length reduces the plasma velocity due to the change in pressure as given in Eq. 2. Thus, the measured specific impulse decreases from 339 to 265 s following the same trend with calculated values in which specific impulse drops from 266 to 212 s following the equation I_S[s] = − 15.03 L[cm] + 310.2.

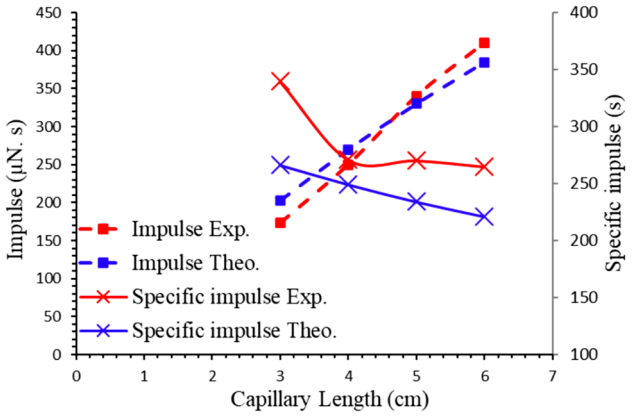

Fig. 14 Change in measured and calculated impulse, and specific impulse with the capillary length

4.3 Capillary radius

Table 2 contains the values of ablated mass of two capillary diameters 4 mm and 6 mm with a fixed length for the capillary of 5 cm and with a discharge current of 1.95kA. The tables addresses the difference of several quantities, such as ablated mass, temperature, heat flux, peak pressure, peak velocity, plasma density, ion density, thrust, impulse, and specific impulse. As the capillary diameter increases from 4 to 6 mm, the capillary volume increases which causes a reduction in energy density reaching the wall leading by a reduction in the temperature from 1.81 eV to 1.57 eV.

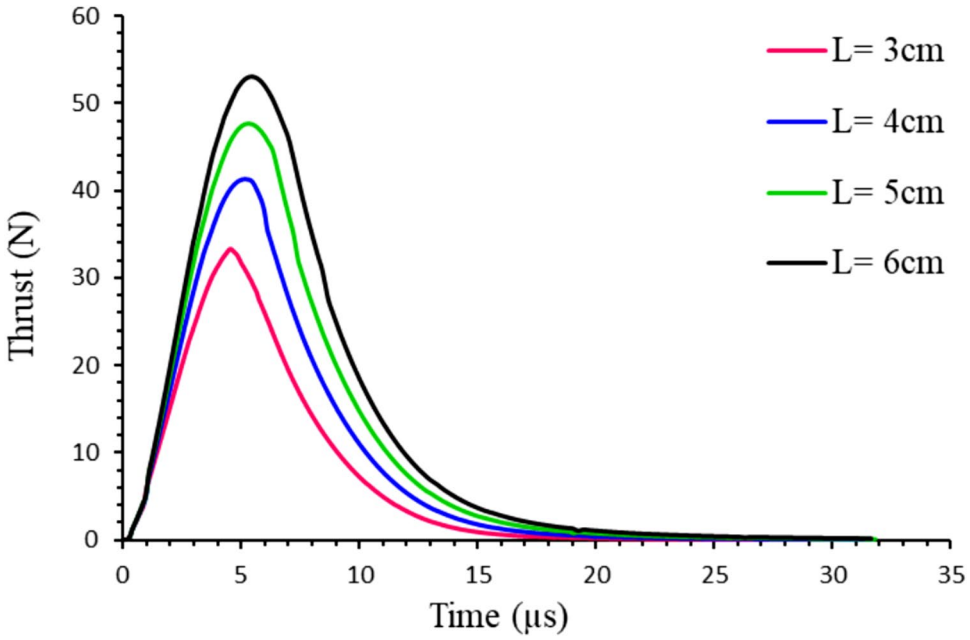

Fig. 13 Thrust profile with different values of capillary length

Table 2 Thrust parameters for different capillary diameters

Diameter (mm)	4 mm	6 mm
Ablated mass experimentally (μg)	128.4	85.2
Ablated mass theoretically (μg)	145	86
Impulse experimentally (μN. s)	340	206
Impulse theoretically (μN. s)	330	187.6
Specific impulse experimentally (s)	270	241.7
Specific impulse theoretically (s)	234	223
Peak temperature (eV)	1.81	1.57
Heat flux (GW/ m^2)	0.63	0.24
plasma density (kg/ m^3)	0.11	0.03
Ion density $\times 10^{23}$ (m^{-3})	5.96	1.66
Peak pressure (bar)	5.13	1.27
Peak velocity (km/s)	2.86	2.7
Thrust (N)	47.6	25.8

According to Eq. 8, the heat flux follows the behavior of temperature, and it also decreases from 0.63 GW/m^2 to 0.24 GW/m^2. According to Eq. 7, the ablated mass decreases with the reduction in heat flux, so it decreases experimentally from 128.4 μg to 85.2 μg accompanied by decreasing in impulse value from 340 μN. s to 206 μN. s.

The reduction in temperature and ablated mass is accompanied by a decrease in ion density and plasma density, consequently reducing the exit pressure as described by Eq. 12. Furthermore, the reduction in temperature reduces the kinetic energy of plasma species, results in a reduction of the exit velocity and, consequently, the thrust, impulse, and specific impulse [8, 12].

According to the previous discussions, as the capillary length increases, the ablation process also increases due to the larger surface area exposed to the radiation heat flux, which in turn leads to an increase in the plasma density, the pressure, and the impulse. In contrast, a reduction in specific impulse is observed due to a decrease in plasma velocity. On the other hand, increasing the capillary radius leads to a reduction in ablated mass and impulse due to the lower heat flux that is incident on the inner wall of the capillary.

4.4 Thrust efficiency

Trust efficiency is defined as the ratio of the kinetic energy gained and the input energy, as expressed by the following equation [30, 31]:

$$\eta = \frac{\frac{1}{2}mv^2}{E_{in}} = \frac{I_m^2}{2mE_{in}} \tag{14}$$

Table 3 shows thrust efficiency as a function of input energy and capillary length. It is shown that, at constant input energy of 6 J, thrust efficiency increases from 4.8 to 8.9% with increasing capillary length from 3 to 6 cm, while for a capillary length of 5 cm, the thrust efficiency is varied between 7.5% and 4.7% as the input energy changed between 6 J and 42.6 J.

Table 3 Thrust efficiency for different values of the input energy and the capillary length

Input energy (J)	Length (cm)	Ablated mass (μg)	Impulse (μN. s)	Thrust efficiency %
6	3	52	173	4.8
6	4	94.2	250	5.5
6	5	128.4	340	7.5
6	6	158	410	8.9
10.6	5	342.6	761.4	7.9
23.9	5	465.8	1021.8	4.7
42.6	5	980.8	2156	5.6

5 Conclusion

An electrothermal PPT experiment was designed with a Teflon capillary. The ablated mass of the propellant was measured for different values of the peak discharge current. By increasing the peak current from 1.95 kA to 5.66 kA, the ablated mass increased from 128.4 μg to 980.8 μg per pulse. In addition, the measured impulse increases from 340 μN.s to 2156 μN.s. Moreover, it was shown that increasing the number of pulses with a current of 1.95 kA, led to an increase in the total ablated mass from 0.064 g after 500 pulses to 1.26 g after 5000 pulses, and the capillary diameter increased from 4 to 5.5 mm. For 1.95 kA, increasing the capillary length from 3 to 6 cm raises the measured ablated mass from 52 μg to 158 μg, the measured impulse from 173 μN.s to 464.5 μN.s, and the measured specific impulse decreases from 339 to 265 s.

The experimental data were compared to calculated data obtained from the ETFLOW model, which describes electrothermal discharge based on fundamental equations, including the continuity equation, momentum equation, and velocity equation. The ablated mass was calculated using the ideal transmission heat factor and the modified one. The results from the modified transmission heat factor equation are more reliable as compared to the experimental results. Also, for a discharge current of 1.95 kA, the calculated ablated mass increased from 79μg to 179 μg, and the impulse increased from 202 μN.s to 480 μN.s by increasing the capillary length from 3 to 6 cm, which agrees with the measured values, while the thrust efficiency increases from 4.8 to 8.9%.

Several discharge properties, such as velocity, heat flux, plasma temperature, and pressure, were analyzed and found

to increase with increasing peak current. In addition, thruster parameters such as thrust, impulse, and specific impulse were also studied as a function of peak current. It was found that, by increasing the peak discharge current from 1.95 to 5.66 kA, the measured impulse increased from 340 μN.s to 2156 μN.s. In contrast, the thrust efficiency is varied in the range between 7.5 and 4.7% as the input energy changed between 6 J and 42.6 J.

Author contributions M. M. Abo El-Hadeed Conducted the experiment, discussed the results, Writing, Data Curing, Formatting, and Review. M. E. Abdelkader Conducted the experiment, Discussed the results, Writing and Review. F. B. Diab Conducted the experiment, Discussed the results, Writing and Review. M. A. Abd Al-Halim Conducted the experiment, Discussed the results, Writing, Data Curing, Formatting, and Review. All authors read and approved the final manuscript.

Funding Open access funding provided by The Science, Technology & Innovation Funding Authority (STDF) in cooperation with The Egyptian Knowledge Bank (EKB). This work has no fund.

Data availability No datasets were generated or analysed during the current study.

Declarations

Conflict of interest The authors declare no competing interests.

Ethical approval The study was conducted according to the guidelines of the Declaration of Benha University and approved by the Ethics Committee of the Faculty of Science, Benha University (Code: BUFS-REC-2024-247Phy).

References

1. Ou, Y., Zhang, Y., Wu, J., Li, J., Tan, S., Zhao, Y.: Comparative study of PTFE filled different dopants as propellants for laser-electric hybrid thruster. Acta Astronaut. **183**, 199–210 (2021). https://doi.org/10.1016/j.actaastro.2021.03.018
2. Gessini, P., Habl, L. T., Barcelos Jr, M. N., Ferreira, J. L., Marques, R. I., & Coletti, M. (2013, October). Low power ablative pulsed plasma thrusters. In Proc. of the 33rd Int. Electric Propulsion Conf.(Washington, DC) (pp. 2013–344).
3. Yang, Z.H.O.U., Ningfei, W.A.N.G., Xiangyang, L.I.U., Ling, W.Y.L., Kan, X.I.E., Zhiwen, W.U.: Experimental investigation on the evolution of plasma properties in the discharge channel of a pulsed plasma thruster. Plasma Sci. Technol **22**(6), 065504 (2020). https://doi.org/10.1088/2058-6272/ab7ed9
4. Aheieva K., Toyoda K., & Cho, M. (2016). Vacuum arc thruster development and testing for micro and nano satellites. *Transactions of the Japan Society for Aeronautical and Space Sciences, Aerospace Technology Japan*, 14(ists30), Pb_91-Pb_97.
5. Zhiwen, W.U., Huang, T., Xiangyang, L.I.U., Ling, W.Y.L., Ningfei, W.A.N.G., Lucheng, J.I.: Application and development of the pulsed plasma thruster. Plasma Sci. Technol **22**(9), 094014 (2020). https://doi.org/10.1088/2058-6272/aba7ac
6. Bushman, S.S., Burton, R.L.: Heating and plasma properties in a coaxial gasdynamic pulsed plasma thruster. J. Propul. Power **17**(5), 959–966 (2001). https://doi.org/10.2514/2.5849
7. Zhang, Z., Ling, W.Y.L., Tang, H., Cao, J., Liu, X., Wang, N.: A review of the characterization and optimization of ablative pulsed plasma thrusters. Rev. Modern Plasma Phys. **3**, 1–41 (2019). https://doi.org/10.1007/s41614-019-0027-z
8. Wang, Y., Ding, W., Cheng, L., Yan, J., Li, Z., Wang, J., Wang, Y.: An investigation of discharge characteristics of an electrothermal pulsed plasma thruster. IEEE Trans. Plasma Sci. **45**(10), 2715–2724 (2017). https://doi.org/10.1109/TPS.2017.2738330
9. Wang, Y., Ding, W., Le Cheng, J. Y., Li, Z., & Shen, S. (2017). A novel pulsed plasma thruster design based on special capillary cavity structure.
10. Edamitsu, T., Asakura, H., Matsumoto, A., & Tahara, H. (2005). Research and development of a pulsed plasma thruster in Osaka University. In 29th International Electric Propulsion Conference.
11. Ou, Y., Wu, J., Du, X., Zhang, H., He, Z.: Experimental investigation on characteristics of pulsed plasma thrusters with the propellant samples of modified PTFE filled Si, Al and Al2O3. Vacuum **165**, 163–171 (2019). https://doi.org/10.1016/j.vacuum.2019.04.027
12. Edamitsu, Toshiaki, Hirokazu Tahara, and Takao Yoshikawa. Performance characteristics of a coaxial pulsed plasma thruster with Teflon cavity.In Proceedings of the Korean Society of Propulsion Engineers Conference, pp. 577–587. The Korean Society of Propulsion Engineers, (2004).
13. Uezu, J., Iio, J., Kamishima, Y., Takegahara, H., Wakizono, T., & Sugiki, M. (2005, October). Study on pulsed plasma thruster configuration to expand impulse bit range. In 29th International electric propulsion conference (Vol. 234).
14. Keidar, M., Boyd, I.D.: Ablation study in the capillary discharge of an electrothermal gun. J Appl Phys (2006). https://doi.org/10.1063/12174111
15. Keidar, M., Boyd, I.D., Beilis, I.I.: Model of an electrothermal pulsed plasma thruster. J. Propul. Power **19**(3), 424–430 (2003)
16. Cambier, J., Marcus Young, Leonid Pekker, and Anthony Pancotti. "Capillary discharge based pulsed plasma thrusters." In International Electric Propulsion Conference, pp. 2007–238. 2007.
17. Abdel-Kader, M.E., Abd Al-Halim, M.A., Bourham, M.A.: Generation of noble and refractory metals plasma jets by electrothermal discharge for surface deposition applications. IEEE Trans. Plasma Sci. **46**(6), 2099–2107 (2018). https://doi.org/10.1109/TPS.2018.2829108
18. Abd Al-Halim, M.A., Bourham, M.A.: Effect of dimensional changes on plasma characteristics in electrothermal capillary discharges for optimized performance in fusion pellet injection. Plasma Phys. Rep. **44**, 870–877 (2018). https://doi.org/10.1134/S1063780X18090015
19. Mohanti, R.B., Gilligan, J.G.: Time dependent simulation of the plasma discharge in an electrothermal launcher. IEEE Trans. Magn. **29**(1), 585–590 (1993). https://doi.org/10.1109/20.195641
20. Winfrey, A.L., Abd Al-Halim, M.A., Gilligan, J.G., Saveliev, A.V., Bourham, M.A.: A study of plasma parameters in a capillary discharge with calculations using ideal and nonideal plasma models

for comparison with experiment. IEEE Trans. Plasma Sci. **40**(3), 843–852 (2012). https://doi.org/10.1109/TPS.2011.2179985
21. Hurley, J.D., Bourham, M.A., Gilligan, J.G.: Numerical simulation and experiment of plasma flow in the electrothermal launcher SIRENS. IEEE Trans. Magn. **31**(1), 616–621 (1995). https://doi.org/10.1109/20.364624
22. Abo El-Hadeed, M. M., Bourham, M. A., and Abd Al-Halim, M. A., "Modeling of Thrust Properties for Capillary-Type Pulsed Plasma Thrusters Using Electrothermal Discharge in Teflon." IEEE Transactions on Plasma Science (2024).
23. Abd Al-Halim, M.A., Bourham, M.A.: Characterization of short intense pulsed electrothermal plasma capillaries for use as fusion and launchers heat flux sources. J. Fusion Energy **33**, 258–263 (2014). https://doi.org/10.1007/s10894-014-9664-y
24. Echols, J.R., Winfrey, A.L.: Ablation of fusion materials exposed to high heat flux in an electrothermal plasma discharge as a simulation for hard disruption. J. Fusion Energy **33**, 60–67 (2014). https://doi.org/10.1007/s10894-013-9639-4
25. Gilligan, J., Hahn, D., Mohanti, R.: Vapor shielding of surfaces subjected to high heat fluxes during a plasma disruption. J. Nucl. Mater. **162**, 957–963 (1989). https://doi.org/10.1016/0022-3115(89)90393-0
26. Gilligan, J.G., Mohanti, R.B.: Time-dependent numerical simulation of ablation-controlled arcs. IEEE Trans. on Plasma Sci. **18**(2), 190–197 (1990). https://doi.org/10.1109/27.131019
27. Schoenherr, T., & Komurasaki, K. (2011). Pulsed Plasma Thrusters: a worldwide review and long yearned classification.
28. Marquart, E., & Coulter, S. (1998, January). Impulse measurement technology development at the Arnold Engineering Development Center (AEDC). In 36th AIAA. https://doi.org/10.2514/6.1998-203
29. Muller, L.: Modelling of an ablation controlled arc. J. Phys. D Appl. Phys. **26**(8), 1253 (1993). https://doi.org/10.1088/0022-3727/26/8/015
30. Antropov, N. N., Popov, G. A., Kazeev, M. N., Chesta, E., & Khodnenko, V. P. (2007). Low bank energy APPT for micro satellites. In 30th International Electric Propulsion Conference, Florence, Italy (pp. 17–20).
31. Wang, Z., Eun, Y., Wu, X.: Design and demonstration of a micro air-fed magnetoplasmadynamic thruster for small satellites. Acta Astronaut. **181**, 482–491 (2021). https://doi.org/10.1016/j.actaastro.2021.01.047